

## Research Article

# Gas Network Development in Compact Bentonite: Key Controls on the Stability of Flow Pathways

J. F. Harrington <sup>1</sup>, C. C. Graham,<sup>1</sup> R. J. Cuss,<sup>1</sup> and S. Norris<sup>2</sup>

<sup>1</sup>British Geological Survey, UK

<sup>2</sup>Radioactive Waste Management Ltd., UK

Correspondence should be addressed to J. F. Harrington; [jfha@bgs.ac.uk](mailto:jfha@bgs.ac.uk)

Received 18 June 2018; Revised 15 August 2018; Accepted 28 August 2018; Published 20 May 2019

Academic Editor: Reza Rezaee

Copyright © 2019 UK Research & Innovation (UKRI). This is an open access article distributed under the Creative Commons Attribution License, which permits unrestricted use, distribution, and reproduction in any medium, provided the original work is properly cited.

Compacted bentonite is proposed as an engineered barrier material within facilities for the geological disposal of radioactive waste. Barrier performance and its interaction with a free gas phase must be considered as part of sound repository design. This study involved the long-term experimental examination of gas flow in precompacted bentonite, with particular consideration of gas network stability. Results demonstrate that the stress field experienced by the clay is strongly coupled with gas flow. For the first time, three controls on this behaviour are considered: (i) injection flow rate, (ii) constant vs. variable gas pressure, and (iii) stimulation of the microfracture network. A detailed stress analysis is used to examine changes in the gas flow network. The results indicate a degree of metastability despite these changes, except in the case of stimulation of the microfracture network by removal of the primary drainage route. In this case, a rapid redevelopment of the gas flow network was observed. As such, availability of drainage pathways will represent a key control on the generation of peak gas pressures and distribution of gas within the engineered barrier. The cessation of gas flow is shown to result in crack closure and self-sealing. Observations from this study highlight that characterisation of the gas network distribution is of fundamental importance in predicting gas dissipation rates and understanding the long-term fate of gas in radioactive waste repositories.

## 1. Introduction

Understanding the subsurface movement of gas is of primary importance for a host of geoscience applications from petroleum engineering to radioactive waste disposal. In all geological scenarios, gas movement may occur through the combined processes of molecular diffusion (governed by Fick's Law), solubility (Henry's Law), and bulk advection [1]. However, in many natural and engineering scenarios, the background diffusion of gas is too slow to remove sufficient mass from the system. As gas generation continues and the gas dissolved in the adjacent porewater exceeds the solubility limit, a free gas phase forms within the pore space of the rock [2–5]. Gas continues to accumulate until advective transport occurs. In reality, the rate of gas flux and the mechanisms governing its movement through a particular formation are, therefore, controlled by the rate of gas production.

In porous media, the advection of gas is generally described by combining the continuity equation with the generalised form of Darcy's Law and constitutive equations for relative permeabilities and capillary pressures between phases [6]. To complete the description of the system, it is necessary to define the relative permeabilities and capillary pressures as functions of the phase saturations. These may be defined either with tabulated data or explicit functional forms such as van Genuchten [7] and may also incorporate hysteretic effects [8].

However, the application of such an approach to compact bentonite is called into question, since swelling clays differ from other porous media by a number of distinguishing features. These include the submicroscopic dimensions of the interparticle spaces [9], the large surface area of the mineral substrate [10], strong physicochemical interactions between porewater and substrate [11, 12], low permeability [13], a deformable matrix leading to a pronounced coupling between the hydraulic and mechanical responses, and a low

tensile strength [14]. These characteristic attributes, common to all clay materials, confluent such that the capillary pressure required to initiate gas flow is too large for the gas to penetrate and desaturate the clay [15]. Under these circumstances, dilatancy can occur [16]. Here, gas transport is not directly governed by permeability tensors or phase saturations but by a complex hydromechanical coupling between the gas pressure and stress state [17]. In addition, studies examining the degree of instability in immiscible flow systems highlight that even in idealised, smooth, and parallel plate fractures, flow is both localised and unstable [18]. However, very little work examining this behaviour is available in the literature.

In a porous material, the state of stress can be described as a tensor quantity,

$$\sigma_{ij} = \sigma_{ij}^e + \alpha \delta_{ij} P_p, \quad (1)$$

where  $\sigma_{ij}^e$  is the effective stress resulting from the opposing pore pressure,  $P_p$ , the Biot parameter,  $\alpha$ , and the Kroekner delta. For simplicity, this is commonly reduced to the consideration of three perpendicular principal stresses. For clays and shales with sufficiently narrow pore throats and a low tensile strength, the conditions necessary for gas fracture may be reached before capillary flow is viable [1]. In such a scenario, an upper bound on gas pressure is given by the minimum principal stress acting on the porous mass. When gas pressure approaches and exceeds this stress vector, deformation of the fabric occurs as gas penetrates and propagates through the material, creating dilatant microfractures [15, 19–25]. Understanding the impact of the gas pressure gradient on the mass transfer rate of gas and changes in drainage configuration on the distribution of gas flow, gas pressure, and stress within the subsurface is of fundamental importance.

In a heat-emitting repository for radioactive waste, the issue of gas transport and its impact on repository infrastructure is a key factor in performance assessment (PA). Central to these considerations is the response of the low permeability engineered (montmorillonite-based) barrier systems (EBS). These materials are used to isolate the waste and seal both galleries and shafts. However, following closure and rehydration of the repository, anaerobic degradation of waste, metal components, and radiation of porewater occur, leading to the formation of a free gas phase [16]. While significant effort has been placed on examining the fate of this gas as it initially migrates through the clay [26], little attention has been placed on the sensitivity of gas flow to changes in boundary condition. In addition, there is little information regarding the long-term stability and controls on gas flow behaviour in compact bentonite. In order to address this issue, a long-term experiment is described examining the impact of changing boundary condition on a preestablished network of conductive gas pathways, their stability, and their temporal and spatial evolution within the clay. To simulate the scenario of a radioactive waste canister hosted in a hard rock repository, testing is conducted in a constant volume apparatus that mimics the properties of an unyielding host rock wall. Gas migration within this test has been shown to occur through an induced network of localised pathways

[17], which is consistent with direct observations using nanoparticle traces (Harrington et al., 2012). This paper describes three experimental scenarios examining (i) flow rate control on the mobility of gas, (ii) influence of boundary condition on the stability of gas pathways, and (iii) stimulation of the microfracture network. A new stress analysis technique is applied to the resulting dataset and implications for radioactive waste disposal discussed.

## 2. Apparatus, Material, and Test Stages

In line with repository concepts hosted in a hard rock (crystalline) geology, the specimen was volumetrically constrained, preventing dilation of the clay in any direction. This British Geological Survey (BGS) custom-designed apparatus has six main components: (1) a thick-walled, dual-closure stainless steel pressure vessel; (2) an injection pressure system; (3) three independent back pressure systems; (4) five total stress gauges to measure radial and axial total stresses; (5) a porewater pressure monitoring system; and (6) a microcomputer-based data acquisition system. The pressure vessel was comprised of a dual-closure tubular vessel manufactured from 316 stainless steel and pressure-tested at 69 MPa. Each of the end closures had a large filter embedded in its surface (denoted either EC-1 or EC-2) and was secured by twelve high tensile cap screws which could also be used to apply a small prestress to the specimen if required.

The 60 mm internal bore of the pressure vessel was honed to give a highly polished surface. All ports, except those for the direct measurement of stress, contained sintered porous plugs, profiled to match the bore of the pressure vessel. The stress gauges were designed in-house using a 10.0 mm tungsten carbide pushrod fitted with an “O”-ring seal. These acted directly upon a load cell mounted on the external surface of the vessel. The layout of the stress and pressure sensors is shown in Figure 1(a). The axial total stress sensors are denoted A1 and A2 while the three radial sensors are labelled R1, R2, and R3. The central or “source” filter was embedded at the end of a 6.4 mm diameter stainless steel tube and was used to inject the permeant, in this case, helium. The end of the filter was profiled to match a standard twist drill.

Pressure and flow rate of test fluids were controlled using four ISCO, syringe pumps, operated by two independent control units. Movement of the pump piston was controlled by a microprocessor which continuously monitored and adjusted the rate of rotation of the encoded disc using a DC motor connected to the piston assembly via a geared worm drive. This allowed each pump to operate in either constant pressure or constant flow modes.

Given the potential for gas leakage past the injection pump seal, a constant flow rate was applied by displacing the gas from a precharged interface vessel (Figure 1(b)). This helped to ensure that the helium was water saturated prior to injection, reducing the potential for desiccation. A programme written in LabView™ elicited data from the pump at preset time intervals, generally 120 s. Testing was performed in an air-conditioned laboratory at a nominal temperature of  $20 \pm 0.5^\circ\text{C}$ .

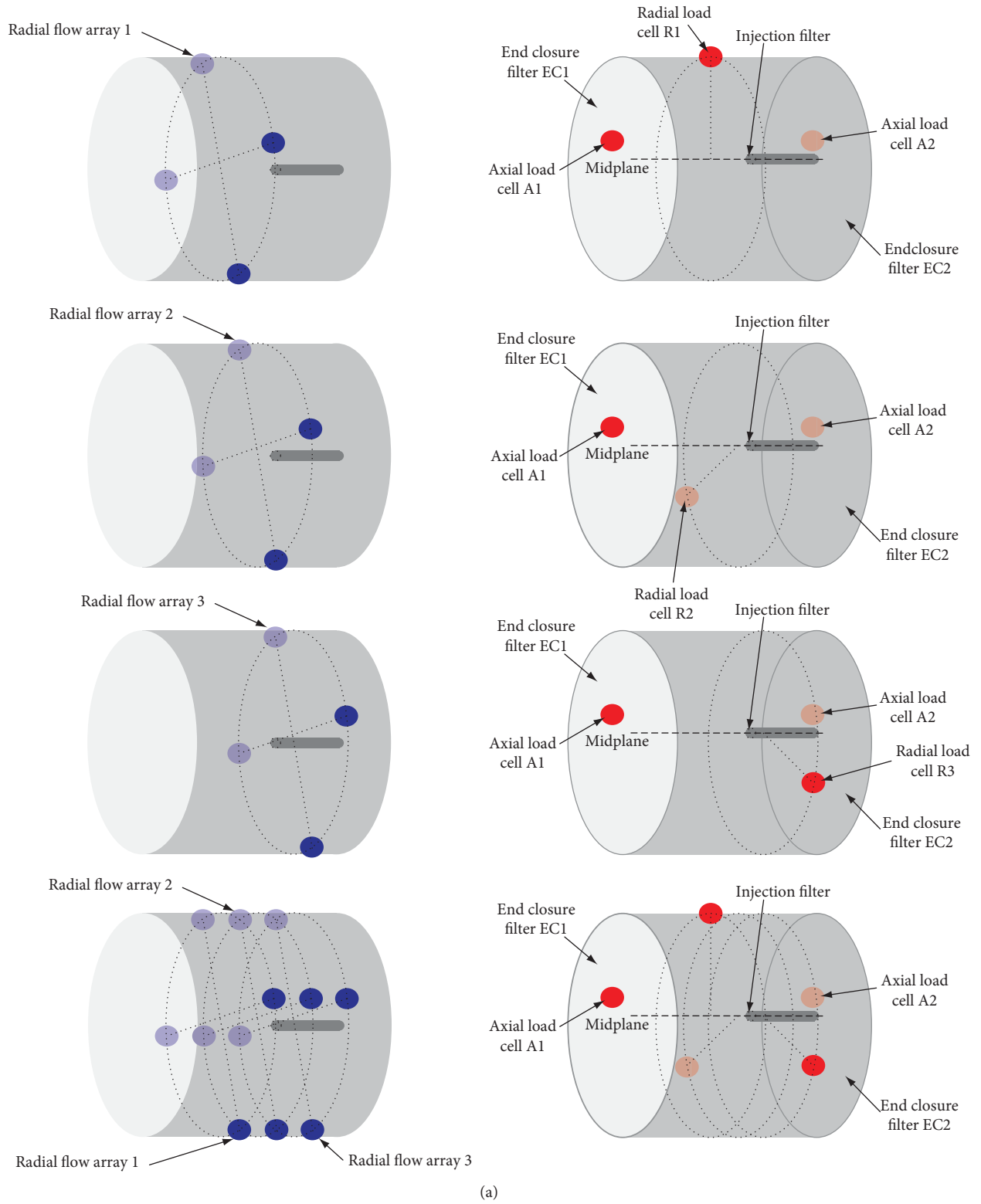


FIGURE 1: Continued.

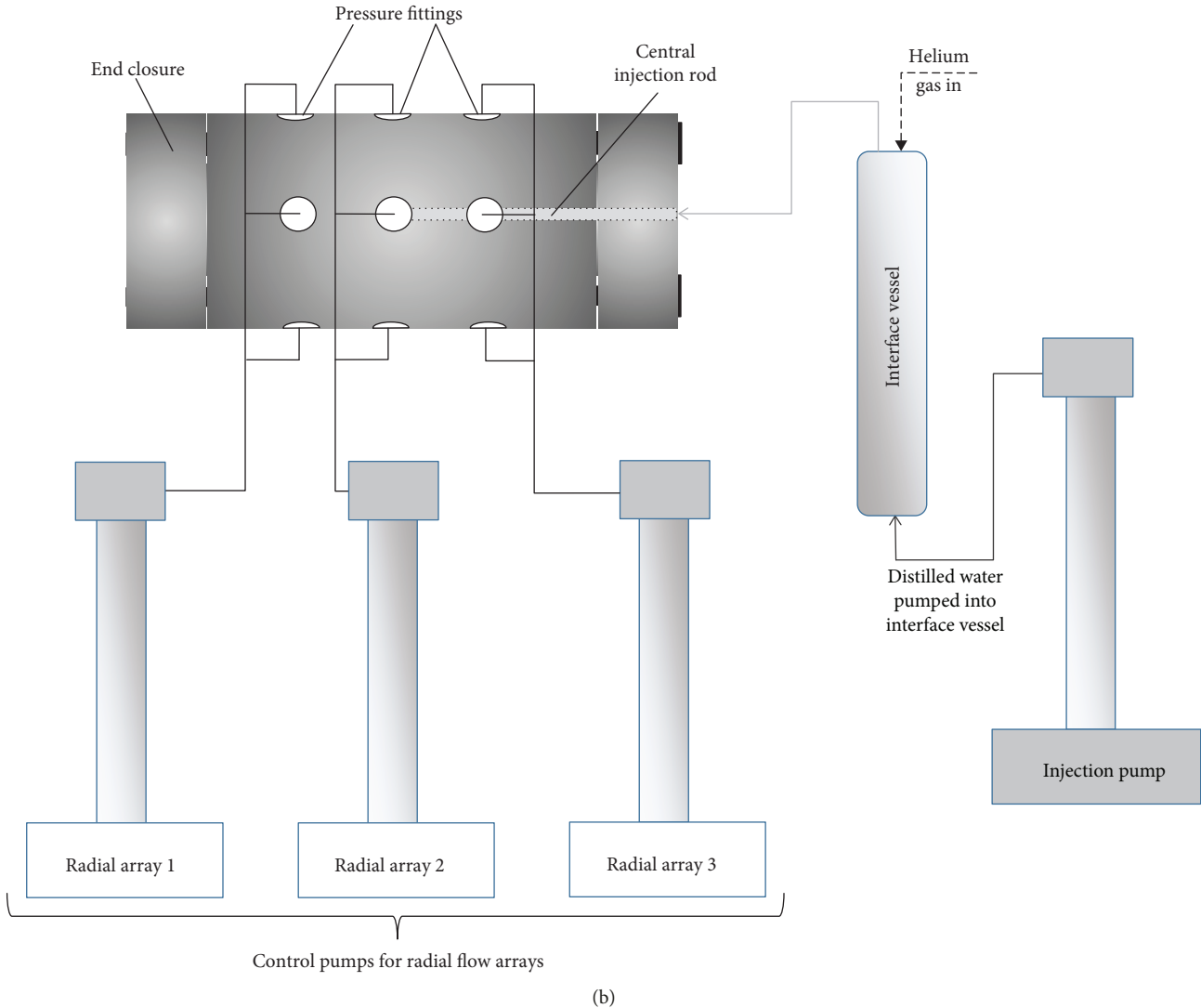


FIGURE 1: (a) Schematic of apparatus showing filter and total stress sensor locations. Each radial flow array comprises four filters (blue dots) set at  $90^\circ$  to each other. Five total stress sensors (red dots) located around the periphery of the sample, two axial and three radial. (b) Schematic showing layout of key apparatus components.

All the sensors were calibrated against laboratory standards by applying incremental steps in pressure, from atmospheric to a predetermined maximum value. This was followed by a descending history to quantify any hysteresis. Least squares fits were calculated and the regression parameters used to correct raw data.

The test sample (designated Mx80-A) came from a precompacted block of Volclay Mx80 bentonite with a nominal dry density of  $1560 \text{ kg}\cdot\text{m}^{-3}$ . The material was supplied by AMCOL International Corporation USA and was type Mx80 from Wyoming. While a detailed analysis of its chemical composition can be found in Johannesson [27], on average, the material comprised (by percentage weight) 90.2% montmorillonite, 0.5% gypsum, 4.8% quartz, 0.1% calcite, 3.5% plagioclase, and 0.9% muscovite. The specimen was manufactured by a combination of dry sawing and machine lathing, resulting in a high-quality specimen with dimensions of the order of 60 mm in diameter

and 120 mm in length. A central hole 6.4 mm in diameter was then drilled from an end face to the midplane of the sample in order to accommodate the injection rod and filter. Pre- and posttest geotechnical properties were determined from the oven drying of offcut material at  $105^\circ\text{C}$  (Table 1).

The initial test stages [1] through [11] are described in detail by Harrington et al. [17] which focussed on the processes governing resaturation, gas entry, and the establishment of steady-state gas flow. In contrast, this paper primarily focusses on post gas breakthrough data from the same test, Mx80-A, designed to examine the impact of variable gas pressure gradient to the mass transfer rate of gas and changes in drainage configuration on the distribution of gas flow, pressure, and stress within the bentonite (Table 2). For clarity, all new stages reported in this paper are labelled alphabetically to distinguish them from those presented by Harrington et al. [17].

TABLE 1: Pre- and posttest geotechnical properties for test sample Mx80-A. Values are based on a grain density of  $2770 \text{ Mg/m}^3$  [29]. Swelling pressure and *intrinsic* permeability are estimated from the saturated void ratio using published trends by Børgesson et al. [36].

	Length (mm)	Diameter (mm)	Moisture content (%)	Porosity (%)	Dry density ( $\text{kg/m}^3$ )	Bulk density ( $\text{kg/m}^3$ )	Saturation (%)	Swelling pressure (MPa)	Intrinsic permeability ( $\text{m}^2$ )
Pretest	121.4	59.8	26.6	43.7	1560	1975	95	8.6	$5.5 \times 10^{-21}$
Posttest	121.7	60.1	28.2	44.2	1545	1981	99	6.5	$5.5 \times 10^{-21}$

TABLE 2: Summary of experimental history showing the test stage, the elapsed time in days at the start of each test stage, injection flow rate, injection pressure, and back pressure. Types of tests are CFRT = constant flow rate test; PDT = pressure decay test; CPT = constant pressure test.

Test stage	Type	Time (days)	Flow rate ( $\mu\text{l/h}$ )	Injection pressure (MPa)	Back pressure (MPa)	Notes
[A]	CFRT	720.3	125	—	1.0	—
[B]	CFRT	838.3	63	—	1.0	—
[C]	CFRT	855.2	31.5	—	1.0	—
[D]	PDT	866.6	0	—	1.0	Injection pump stopped
[E]	CFRT	884.2	31.5	—	1.0	—
[F]	CFRT	898.4	63	—	1.0	—
[G]	CFRT	945.0	126	—	1.0	—
[H]	CPT	948.3	—	7.86	1.0	—
[I]	CFRT	1016.4	171	—	1.0	—
[J]	CFRT	1084.3	171	—	1.0	Radial flow array 3 isolated
[K]	PDT	1161.7	0	—	1.0	Injection pump stopped

### 3. Results

**3.1. Flow Rate Control on the Mobility of Gas.** Prior to the start of testing, the sample was fully saturated before a conductive network of gas pathways was established through the sample using a combination of constant flow rate and constant pressure testing [17]. During test stage [A], Figure 2, gas flow into the system was in quasi-steady-state with 98.9% of the flow focussed primarily through radial array 3. Closer inspection of the data indicates a small amount of gas was also distributed to arrays 1 (0.1%) and 2 (1%). However, at day 826.5, flow spiked in array 2, then decayed to a zero flow condition by around day 835. This event was accompanied by a small increase in stress which then continued to decay for the remainder of the stage. From around day 835 onwards, 100% of the flow occurred purely through radial array 3. This evolution in flow suggests an instability in the flow pathways which continued to spatially and temporally evolve while gas flowed.

The injection flow rate was then halved at day 838.3 (stage [B]) and again at day 855.2 (stage [C]). Tabulated values for flow and pressure are presented in Table 3. Fluxes in and out of the sample quickly decline to a new asymptote. The speed at which this occurs is symptomatic of a fractured system with minimal gas storage within the sample [28]. This is supported by previous data which indicate little if any desaturation of the clay occurs during gas flow [15]. In conjunction with the change in flow, injection pressure also declines though the decrease in pressure is relatively small.

In order to estimate the capillary threshold pressure, the injection pump was stopped, stage [D], and the pressure

allowed to decay. While outflow to radial array 3 quickly declined to a zero flow condition, the injection pressure displayed a fairly linear decay (Figure 2(a)). No significant changes in outflow were observed to either of the other radial arrays (Figures 2(b)–2(d)) which suggests the continued decline in the gas pressure may reflect a small residual leak in the test system. However, this seems somewhat counterintuitive given the mass balance observed in test stages [A] through [C], which indicates that if present, the leakage rate of gas is very small.

During this initial stage of testing, total stress and pressure within filter EC-2 exhibit a general correlation with gas pressure (Figure 3). The general decline in stress and gas pressure continues in stage [D]. In contrast, pressure in filter EC-1 shows a small but gradual increase in pressure during this time (Figure 3(a)). This response and the general lack of “noise” in the data are not symptomatic of previous advective gas flow events. Previous scoping calculations by Harrington et al. [17] suggest that as water in the filter becomes saturated with dissolved gas, continued diffusion could lead to the formation of a free gas phase and indirect pressurisation of the filters. Alternatively, it could be a hydrodynamic effect as water is displaced from the radial filters during gas flow.

In an attempt to reinitiate a network of conductive gas pathways through the sample, the injection pump was switched back to the constant flow rate mode, stage [E], and pumping restarted at a rate of  $31.5 \mu\text{l/h}$ . This resulted in a small drop in gas pressure, then a persistent increase (Figure 2(b)), as the gas was unable to establish a connection to any of the radial filters. With no significant outflow

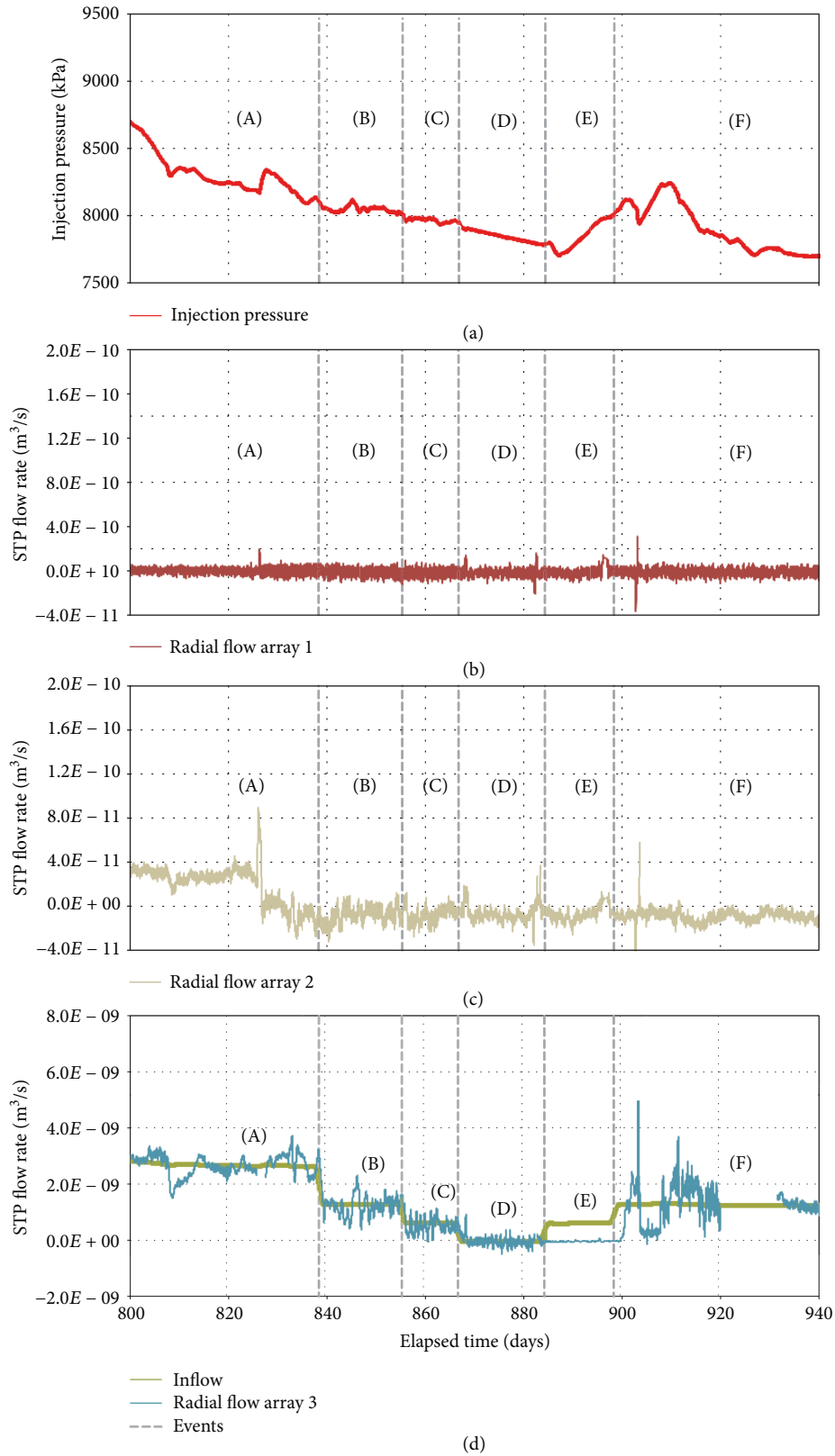


FIGURE 2: Time series data from days 800 to 940 inclusive, showing (a) injection pressure, (b) radial flow to array 1, (c) radial flow to array 2, and (d) inflow and radial flow to array 3. Events highlight changes in boundary conditions signified by the dotted grey lines. Flow data has been corrected to STP and time-averaged to remove noise and highlight underlying trends. Letters in brackets represent individual test stages. The small negative flow in (c) may stem from a small leak from the control system, but this represents less than 0.9% of the total flux measured out of the sample and has no bearing on the interpretation of the data.

TABLE 3: Summary of gas transport properties showing inflow, outflow, injection, and back pressure during quasi-steady-state flow.

Test stage	Inflow (m <sup>3</sup> /s) at STP	Injection pressure (MPa)	Back pressure (MPa)	Outflow at STP radial array 1 (m <sup>3</sup> /s)	Outflow at STP radial array 2 (m <sup>3</sup> /s)	Outflow at STP radial array 3 (m <sup>3</sup> /s)
[A]	$2.49 \times 10^{-9}$	8.12	1.00	$1.6 \times 10^{-12}$	~0	$2.54 \times 10^{-9}$
[B]	$1.24 \times 10^{-9}$	8.05	1.00	~0	~0	$1.39 \times 10^{-9}$
[C]	$5.76 \times 10^{-10}$	7.96	1.00	~0	~0	$5.58 \times 10^{-10}$
[F]	$1.26 \times 10^{-9}$	7.71	1.00	~0	~0	$1.20 \times 10^{-9}$
[H]	$3.20 \times 10^{-9}$	7.86	1.00	~0	~0	$3.17 \times 10^{-9}$
[J]	$2.84 \times 10^{-9}$	7.69	1.00	$1.85 \times 10^{-9}$	$1.70 \times 10^{-9}$	~0

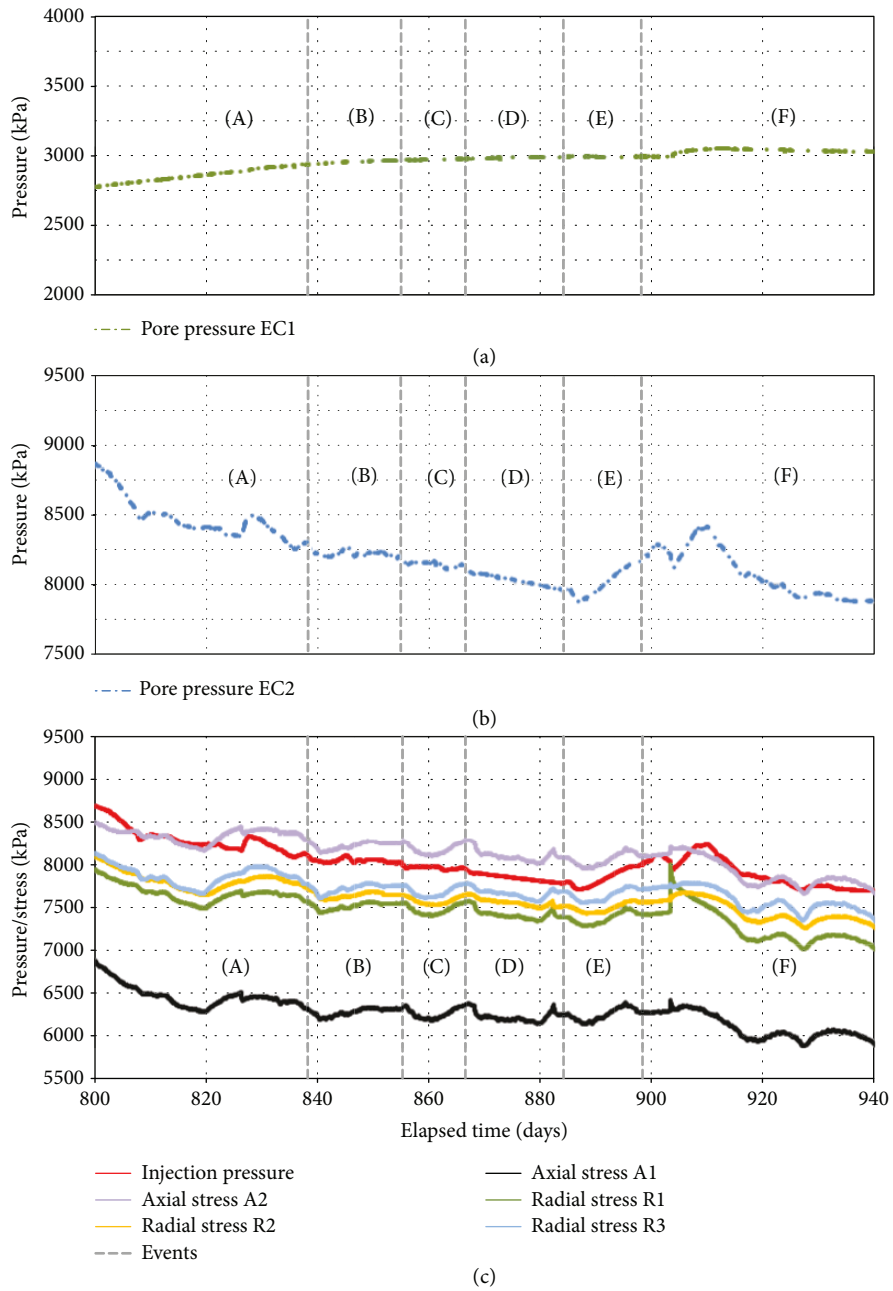


FIGURE 3: Time series data from days 800 to 940 inclusive, showing (a) porewater pressure EC-1, (b) porewater pressure EC-2, and (c) total stress. Letters in brackets represent individual test stages. Events highlight changes in boundary conditions signified by the dotted grey lines.

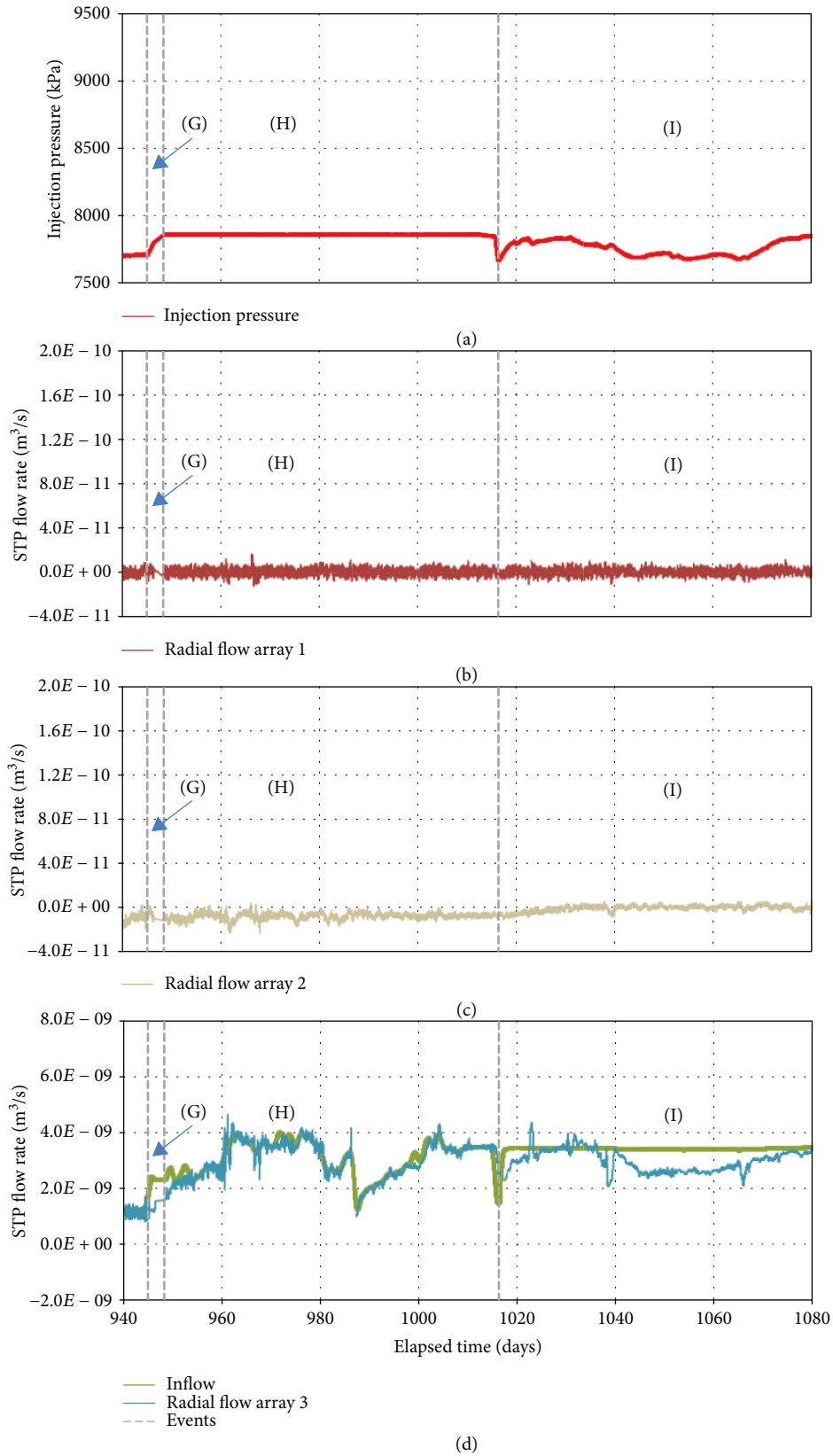


FIGURE 4: Time series data from days 940 to 1080 inclusive, showing (a) injection pressure, (b) radial flow to array 1, (c) radial flow to array 2, and (d) inflow and radial flow to array 3. Events marked by the dotted grey lines highlight changes in boundary conditions. Flow data has been corrected to STP and time-averaged to remove noise and highlight underlying trends. Letters in brackets represent individual test stages.

observed (Figures 2(b)–2(d)), with the exception of a small burst event to all three radial arrays just before the end of stage [E], the injection flow rate was doubled to  $63 \mu\text{l/h}$ , stage [F]. While outflow data is time-averaged and noise removed to illicit the underlying flow behaviour, a clear breakthrough event, signified by the spontaneous discharge of gas to array 3, is observed around day 900 at a peak gas pressure of 8.12 MPa. This was followed by a negative pressure transient until day 903.6, when outflow decreases and the injection pressure begins to increase once more. A second breakthrough event to radial array 3 is subsequently observed with a peak gas pressure of 8.25 MPa recorded. Outflow and gas pressure both exhibit another negative pressure transient reaching a well-defined asymptote by day 936.

Figure 3(c) shows a clear “kick” in radial stress R1 at 903.2 days and is associated with a rapid outburst of gas which occurs just prior to the spontaneous reduction in flow at 903.6 days. This energetic event is also mirrored in radial flow arrays 1 and 2 as a short-lived increase in flow. With the exception of the kick in stress noted above, the remaining load cells appear to continue their general negative trend throughout this period of testing. It is clear from the data that when conductive pathways are present, there is a good correlation between gas pressure, stress, and flow. When pathways cease to be conductive, the correlation can break down as gas pressures then increase, outflow reduces/stops and stress changes are dependent on the magnitude and distribution of the gas pressure within the clay. To examine this further, a detailed numerical analysis of stress events will be presented in Discussion.

**3.2. Influence of Boundary Condition on the Stability of Gas Pathways.** In test stage [G], the flow rate was doubled to  $126 \mu\text{l/h}$  to examine what impact this had on the magnitude and distribution of gas flow. Unfortunately, the data acquisition system crashed leading to a loss of data from day 946 to 948. However, by day 948.3, flow in was approximately equal to flow out (Figure 4(d)).

In order to assess the stability of the pathways, the injection pump was switched to constant pressure mode (set to 7.86 MPa) at the start of stage [H] (Figure 4(a)). This maintained a constant pressure boundary condition while fluxes in and out of the specimen were recorded against time. Figures 4(b)–4(d) show the distribution inflow. For the duration of the test stage, all outflow was focussed through radial array 3; however, the magnitude of the flux can be seen to vary considerably. Even when subject to a static boundary condition, the conductivity of the network of gas pathways changed with time, with flows ranging from  $1.0 \times 10^{-9}$  to  $4.7 \times 10^{-9} \text{ m}^3/\text{s}$  and yielding an average value from day 960 of  $3.2 \times 10^{-9} \text{ m}^3/\text{s}$ .

Towards the end of stage [H], flux appeared to stabilise. To complement these measurements and to assess the sensitivity of injection pressure to a fixed flow rate boundary condition, the stabilised value of flux was selected and the injection pump switched to the constant flow rate mode, stage [I]. Following an initial dip, gas pressures then stabilised at a value close to that imposed in stage [H]. This lasted until around day 1030, when gas pressure began to decrease

and exhibited a greater degree of variability, reaching a minimum and maximum pressure of 7.68 MPa and 7.85 MPa, respectively. This small-scale variability was accompanied by a reduction in outflow to radial array 3 and a very slight increase in flow to radial array 2 (Figure 4). However, by the end of stage [I], injection gas pressure recovered to around 7.85 MPa.

Inspection of the stress and porewater pressure data (Figure 5) during stages [H] and [I] indicates subtle changes occur during these phases of testing. Figure 5(a) shows a slight increase in EC-1 value, though pressure within the filter remains substantially below that of the injection pressure. As seen in Figure 3(a), this increase does not appear to be directly linked to the absolute gas pressure of the injection filter but may be caused by the continued diffusion of gas or a hydrodynamic effect as gas pressures remain above the total stress. Unsurprisingly, the EC-2 pressure trace in Figure 5(b) continues to mimic that of the gas pressure indicating a connection exists from the injection to end closure filters. (Note that a small nonlinear drift in the pressure datum of the injection pump occurred during the course of the test. This resulted in a maximum divergence of only 160 kPa over more than 3 years of the test and explains the discrepancy in pressure between EC-2 and the injection gas pressure.) The response also demonstrates that the drop in gas pressure through the clay is negligible at the scale of these tests. The stress data, presented in Figure 5(c), continues its general negative trend through stages [G] and [H] but then asymptotes early in stage [I]. Analysis of the stress response will be undertaken in Discussion.

**3.3. Stimulation of the Microfracture Network.** The timescales involved in hosting a repository for radioactive waste are substantial, potentially spanning up to 1 Myr. During this time, ground movements and stress conditions are likely to change which may impact the transport properties of the surrounding host rock. In order to assess the impact of such changes on the drainage boundary condition, the pump controlling flow to radial array 3 was stopped, stage [J], preventing further degassing of the clay through these filters. This leads to a spontaneous increase in the injection pressure which was mimicked in both the pressures in radial flow array 3 (Figure 6(a)) and in end closure filter EC-2 (Figure 7(b)). At day 1095, the rate of gas pressurisation markedly reduced. This was caused by a sudden outflow of gas to radial flow array 2 (Figure 6(c)). As gas pressure thereafter continued to increase, flux to array 2 oscillated indicating the newly formed network of conductive pathways was highly unstable and of insufficient aperture to conduct the volumetric flow rate of gas imposed upon the clay. Gas pressure peaked at day 1102, at a value of 11.35 MPa, during which time the outflow to radial flow array 2 continued to show a complex pattern of outflow events. Thereafter, gas pressure began to decline. At day 1115, outflow to radial flow array 1 increased, accompanied by a sharp reduction in flow to array 2. Flux from array 1 gradually decreased with time and, for a short period between days 1124 and 1129, flows in and out of the clay were approximately equal and the gas pressure reached

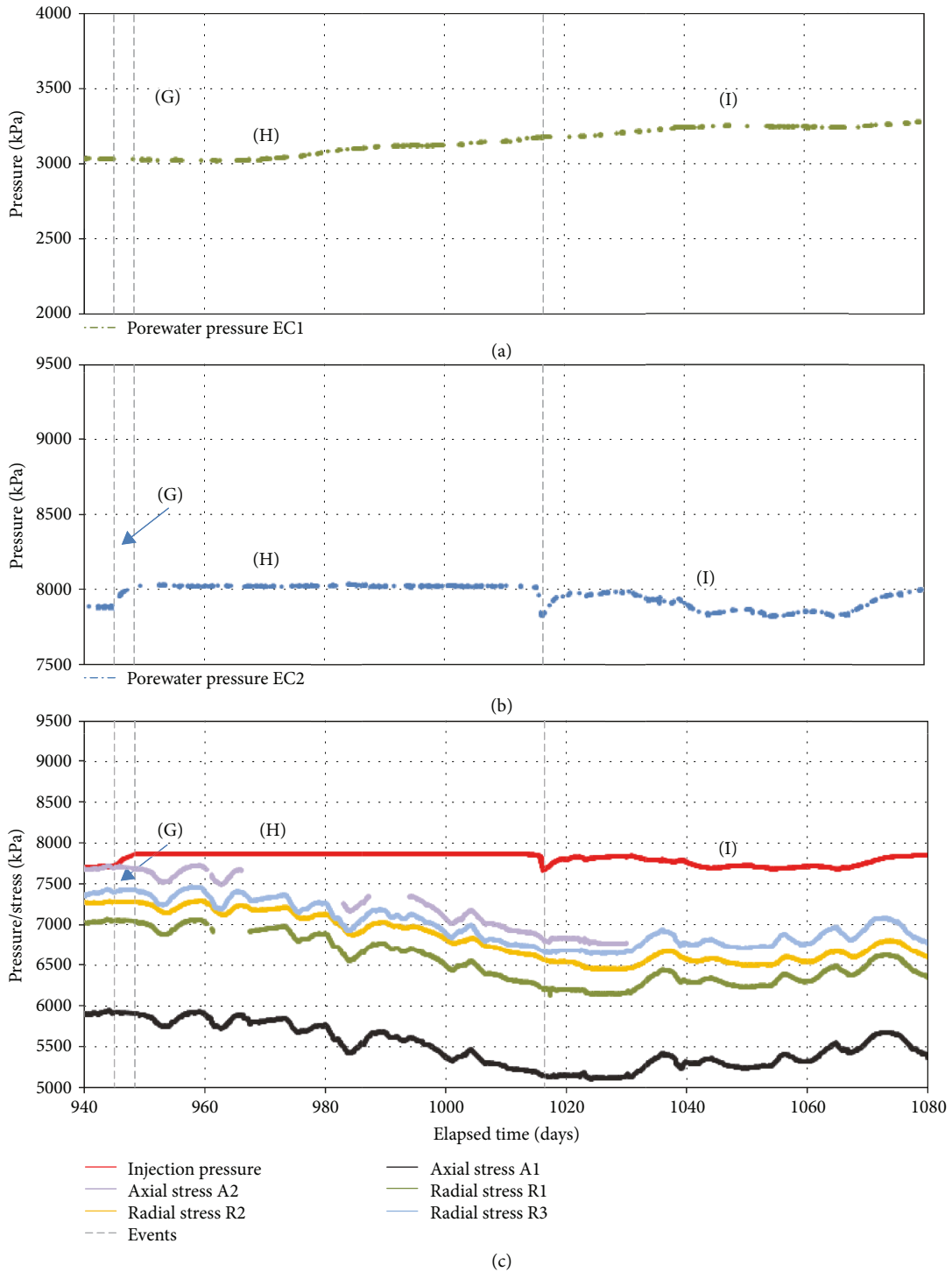


FIGURE 5: Time series data from days 940 to 1080 inclusive, showing (a) porewater pressure EC-1, (b) porewater pressure EC-2, and (c) total stress. Letters in brackets represent individual test stages with events marked by the dotted grey lines representing changes in boundary conditions.

a plateau (Figures 6(a) and 6(d)). This quasi-steady-state is short-lived when a second major discharge event occurred at day 1129, evidenced by a spike in outflow to radial array 1. This was accompanied by a decrease in the injection pressure which began to asymptote towards the end of stage [J]. At this point in the test, fluxes in and out had evolved to be

approximately equal, with 52% of the flux discharged to radial flow array 1 and 48% of flux to radial array 2.

Inspection of the data in Figure 7(a) shows an increase in the pressurisation rate of filter EC-1 at day 1093.7. As the rate of injection pressurisation decreased (noted above), pressure in EC-1 plateaued for a short period of time

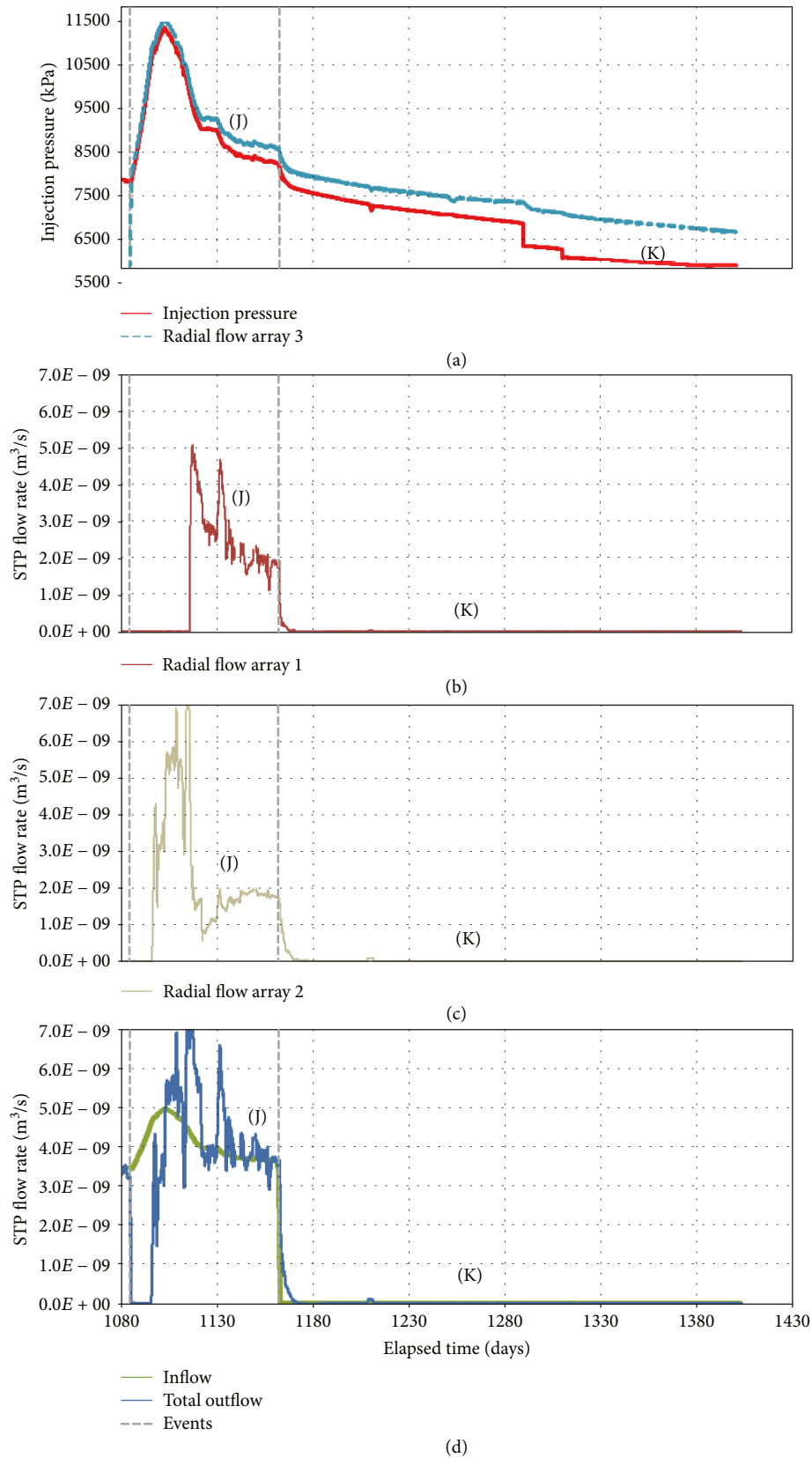


FIGURE 6: Time series data from days 1080 to 1430 inclusive, showing (a) injection and radial flow array 3 pressures, (b) radial flow to array 1, (c) radial flow to array 2, and (d) inflow and total outflow. Events highlight changes in boundary conditions signified by the dotted grey lines. Flow data has been corrected to STP and time-averaged to remove noise and highlight underlying trends. Letters in brackets represent individual test stages.

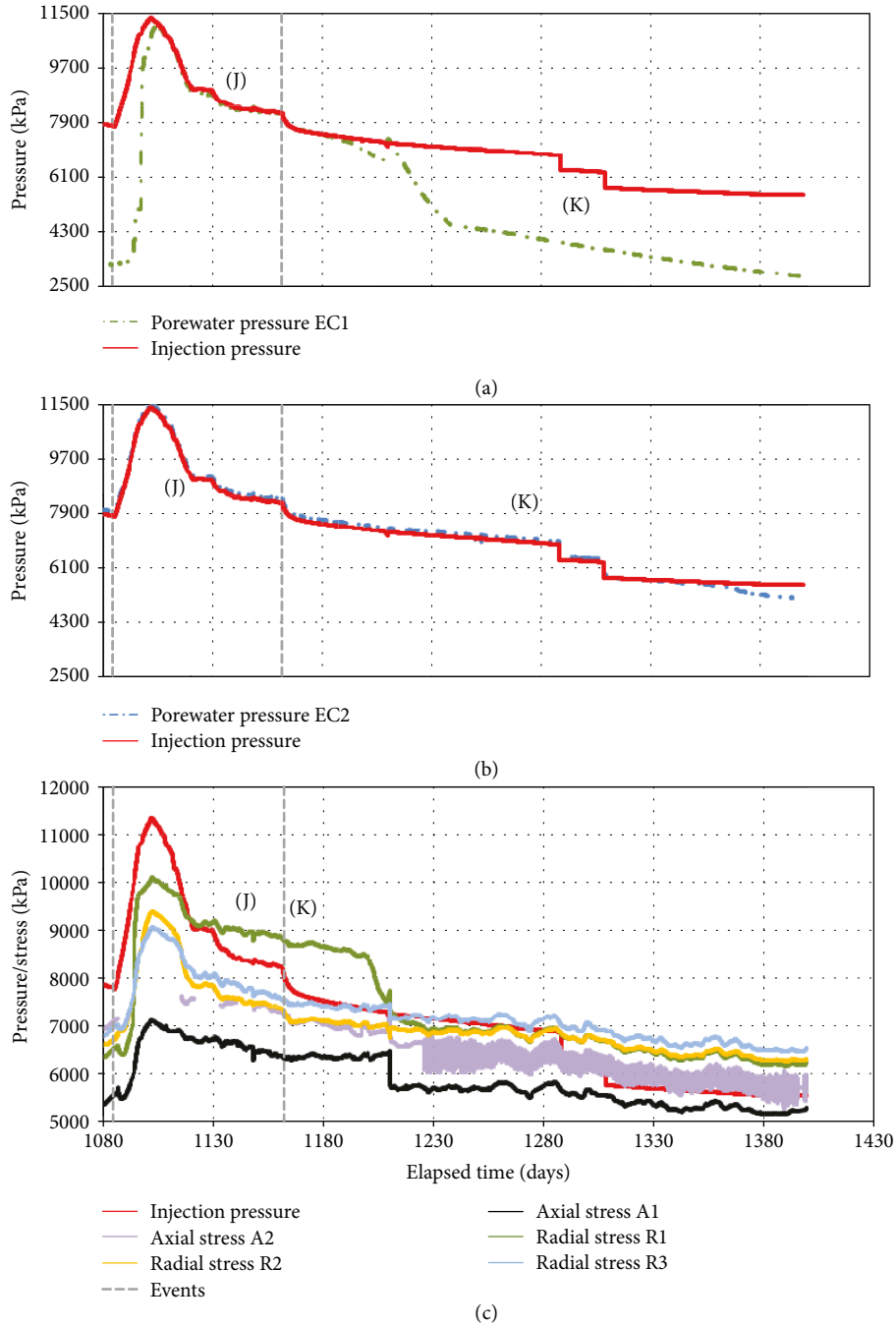


FIGURE 7: Time series data from days 1080 to 1430 inclusive, showing (a) porewater pressure EC-1, (b) porewater pressure EC-2, and (c) total stress. Letters in brackets represent individual test stages.

at a value of 5.07 MPa before rapidly increasing again, as gas pressures continued to increase towards the peak value. From around day 1106, pressure in EC-1 was very close to that of the injection pressure, indicating one or more conductive pathways must have existed between the two points within the sample. During this time, pressure in the other end closure filter (EC-2) was approximately equal to the injection pressure (Figure 7(b)).

Figure 7(c) clearly illustrates the complex coupling between stress, gas pressure, and the development of flow within the clay. As gas pathways connected to the radial

filters, evidenced by discrete outflow events, stress changes were observed. While the stress data will be discussed in detail in Discussion, a number of general observations can be made. Close inspection of Figure 7(c) shows changes in stress occurred shortly after gas pressures began to increase at the start of stage [J]. Localised increases in stress were observed prior to the outflow of gas, indicating both gas penetration of the clay and the development of nonuniformly distributed pathways. As gas pathways continued to develop and flow stabilised towards the end of stage [J], injection pressure and stress response exhibited a clear coupling, the

strength of which is a measure of the number and distribution of conductive pathways within the clay.

The point at which gas ceases to flow within a porous material is referred to as the capillary threshold pressure [29]. To measure this parameter, the injection pump was stopped and gas pressure allowed to decay, test stage [K]. Figure 7 clearly shows that following the cessation of pumping, the flow rate out of the clay rapidly decreases to a slow background level. The exception to this response occurs around day 1210 when a small outburst of gas is noted to both filter arrays.

Careful examination of the data for stage [K] in Figure 7(a) shows a departure occurs between EC-1 and the injection pressure around day 1188. This response indicates closure of the pathway network connecting the two filters. Because of the small gas volume contained within the filter body of EC-1, its pressure then declines at a faster rate than that of the injection pressure. That said, at day 1210 pressure in EC-1 jumps to be equal to gas pressure. This event is accompanied by rapid changes in stress (Figure 7(c)) and the small outflow noted above. However, the conductivity of the pathways connecting EC-1 to the injection filter is short-lived, and they quickly close, evidenced by the decay in EC-1 filter pressure. The rate of decay then reduces around day 1242, thereafter EC-1 decays in an approximately linear fashion.

Gas pressure continued to decrease for the remainder of stage [K]. The two decrements in pressure noted at days 1289 and 1309 were caused by manual adjustments in pressure to remove excess gas from the injection reservoir. This was undertaken to reduce the transient time caused by the nonlinearity of the flow law [15]. This approach worked well and by day 1380 gas pressure and total stress asymptote. This is further supported by the response of EC-2 (Figure 7(b)), which began to diverge from the injection pressure around day 1357 and is symptomatic of pathway collapse. By the end of stage [K], gas pressure had declined to 5.55 MPa, which was similar to the average of all total stress measurements (6.03 MPa).

Upon completion of the test, the sample was removed from the apparatus using a hydraulic jack, measured, and weighed, with the resulting data presented in Table 1. The sample exhibited a slight increase in volume which can be attributed to a combination of swelling to fit the bore of the pressure vessel and stress relaxation when extruded from the apparatus. Even accounting for this change in dimension, the saturation of the sample increased from 95 to 99% by the end of the test. By calculating the average inflow rate between days 800 and 1162, it is possible to calculate the number of litres of gas injected during this phase of testing. Excluding inflow from the previous gas test reported by Harrington et al. [17], the volume of gas injected during this phase of testing was 83.3 litres at STP. This equates to around 560 pore volumes at STP.

## 4. Discussion

*4.1. Stress Field Analysis.* Throughout stages [A] to [K] of gas flow testing, notable fluctuations in the stress field are

detected at multiple sensors. These fluctuations have been observed in previous gas injection experiments on bentonite, conducted under a constant volume boundary condition (Harrington and Horseman, 2003), and have been attributed to the perturbation of the stress field resulting from the dilatant opening and closure of gas flow pathways ([29, 30]). This mechanism provides the best explanation for the stress field behaviour in the experiment presented here. Measured perturbations were seen to occur simultaneously in multiple regions of the clay. One might explain such an observation at an individual sensor by pore pressure fluctuations, but to do so in multiple locations is counter to our understanding of the permeability of bentonite. Any such changes in pore pressure cannot propagate through the clay so rapidly, and clays (including bentonite) are capable of sustaining substantial effective stress gradients for considerable periods of time [31], even of the order of several should over many months. In comparison, translation of the stress field along the length and radius of the sample is relatively instantaneous and can easily explain the events detected. Furthermore, pore pressure evolution is also measured during these experiments. As can be seen in Figures 3 and 5, these sensors do not exhibit an equivalent degree of perturbation observed in the stress field. Some more notable variations are observed for EC-2 in Figure 3; however, close inspection of the data on the daily scale shows that these fluctuations generally follow a perturbation in the stress field, indicating that they are a consequence, not a cause of this behaviour. In the first part of the experiment presented in this study, these perturbations were also observed [17]. Their onset only occurred once gas had entered the clay, highlighting the association between disturbance of the stress field and propagation of pathways caused by gas migration.

Hundreds of these stress fluctuations were noted during this experiment, often detected by multiple load cells in synchronicity. Pressure disturbances generated by inelastic deformation are routinely used to gain insight into the source mechanisms of a number of similar phenomena in geoscience, including earthquakes, microseismics, and acoustic emissions, resulting from fault rupture, hydraulic fracturing, and shear localisation in laboratory experiments, respectively. As such, these perturbations represent an opportunity to derive further information in relation to the development of gas pathways and their subsequent closure. To quantify the degree of stress field disturbance, the first derivative of stress with respect to time ( $d\sigma/dt$ ) was found for each load cell from day 800 (stage [A]) onwards (Figure 8). The magnitude of each resulting derivative is a reflection of the rate at which the stress field is perturbed in the vicinity of that sensor. Before finding the derivative, any initial offset was removed from each stress dataset. Following the same procedure as Harrington et al. [17], a simple “picking” algorithm was used to automatically assess the timing and magnitude of individual stress perturbation events detected at each sensor. In order to discount effects resulting from background noise levels for each sensor, upper and lower thresholds were set, based on the standard deviation (s.d.) of a manually selected “baseline” section of the dataset (consisting of 550 data-points). Selection of the baseline data is described in more

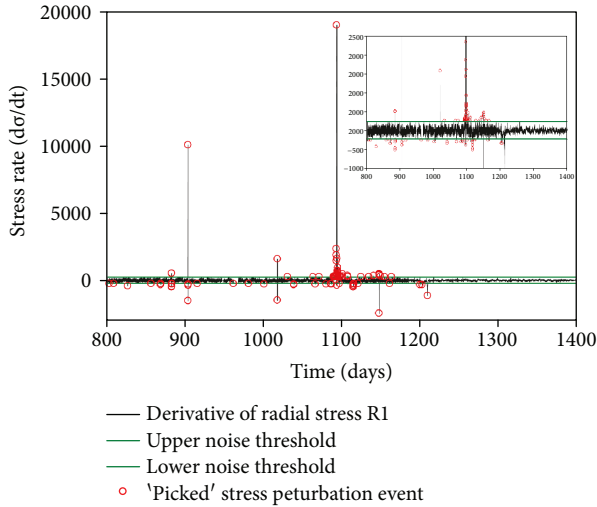


FIGURE 8: Stress event selection for radial stress sensor R1, using the first derivative with respect to time. Perturbations within the upper and lower noise thresholds were automatically excluded.

detail by Harrington et al. [17]. Any rapid changes in the stress field occurring within the noise thresholds were automatically excluded (Figure 8). Maximum and minimum values were then found within a rolling window (3–4 days in length, with an overlap of 1/4 of its length). These values were then compared to previous and subsequent windows in order to select individual peaks and troughs, as highlighted by the red circles in Figure 8. Unlike Harrington et al. [17] who primarily examined events with a positive polarity, here, we also consider those with a negative sign. Similar automatic algorithms are used routinely in seismology (Leonard and Kennett, 1999) and are used as standard practice in the analysis of high-frequency acoustic emissions generated during the microscale fracture of rock in laboratory deformation tests [32, 33]. In this case, the result is a catalogue of stress perturbation “events,” considered to be in excess of background noise levels for each sensor, which highlight periods where development of the stress field is most apparent (Figure 9).

Although this highlights episodes of stress field disturbance as measured in different regions of the clay, it is less instructive in terms of the bulk response of the material to changes in applied gas pressure. In particular, inspection of the timing of events indicates that often the same disturbance is detected by more than one stress sensor. Event detection timings at each sensor were therefore compared in order to generate one combined catalogue of “unique” stress perturbation events. At this stage, it is also important to highlight the importance of temperature on monitored stresses within the clay. Although testing was conducted under temperature-controlled conditions, data from a thermocouple attached to the test vessel showed that a few small excursions in laboratory temperature were observed to coincide with stress perturbation events. As such, the same picking algorithm was used to find the time of all thermal excursion events (above a noise threshold). All stress events found to occur within a period of 1 hour of a temperature excursion were then removed (43 events out of a total of 854).

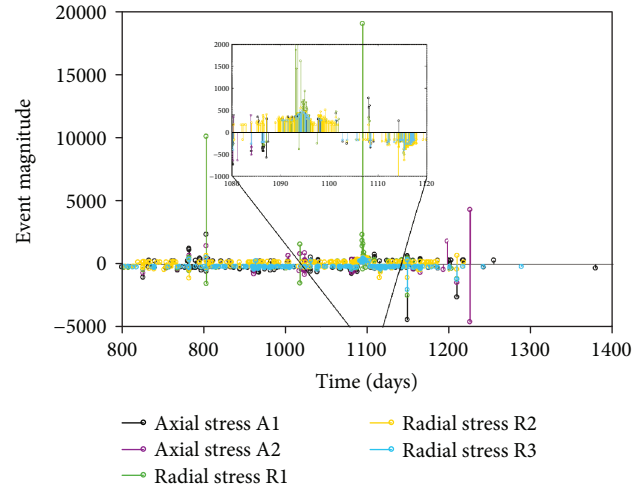


FIGURE 9: Time and magnitude of stress perturbation events detected at each sensor.

The result is a catalogue of timings for unique stress perturbation events, uninfluenced by thermal excursions. In collating the timing of events, it becomes necessary to attribute some measure of magnitude, based on those recorded at different sensors. While much work is required to better understand the source characteristics that generate these stress field disturbances, a number of key controls are likely to influence the detected event magnitude, as with a seismic source, including (i) the amount of energy released during pathway propagation, (ii) the clay’s response to that energy, (iii) the location of the source in relation to the detecting sensor, and (iv) the 3D distribution pattern of energy released. This latter component will be directly related to the geometry of the source and its orientation. Currently, these contributing factors cannot be uncoupled for a number of reasons. Unfortunately, with less than 6 sensors, it is not possible to locate the source of the events in 3 dimensions, and very little can be said about any changes in the bulk clay properties, although some stiffening is thought to occur during microfracture network development resulting from stimulation by mobile gas [34]. Additionally, the aspect ratio and orientation of gas pathways have yet to be characterised [17], meaning that the form of the resulting radiation pattern can only be speculated at.

Nevertheless, it is reasonable to conclude that the event magnitude polarity at a particular sensor is indicative of the radiation pattern in that region of the clay. A positive magnitude will be caused by an increase in local stress, resulting from a greater “opening” component from the source in the direction of that sensor, while a negative magnitude will be caused by a decrease in local stress, resulting from a greater “closing” component from the source in the direction of that sensor. It is therefore possible to infer something about the radiation pattern of the source by considering the averaged magnitude of the source across all detecting sensors. For each unique event, the average was therefore found of measured magnitudes across each stress sensor where a detection occurred, resulting in an “average magnitude” value. While

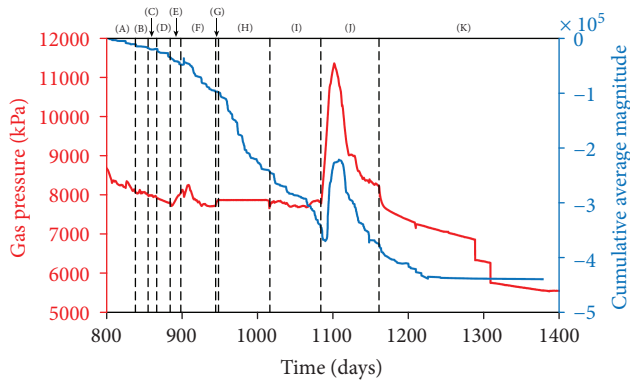


FIGURE 10: Evolution of gas pressure and cumulative average magnitude of stress perturbation events with time. A general trend towards closure is apparent until stage [J] (beginning at day 1084) when large-scale opening correlates with rapidly increasing gas pressure at the time breakthrough occurred. Closure quickly begins to dominate as peak gas pressure is reached and continues after shut-in until stress field perturbation becomes negligible (after day 1300).

this is a crude approach, it provides a “first pass” at source analysis for stress perturbation events and mirrors methodologies used in the early days of source analysis of acoustic emissions in rock fracture experiments [33].

By finding the cumulative sum of the average magnitude of all events with respect to time, an insight can be gained into the degree of pathway “opening” versus “closing” that has occurred up to that point within the clay (Figure 10). The results indicate that the majority of the test was dominated by stress events with a “closure” type of signature, except at the time the major breakthrough occurred (stage [J]) where a significant opening component to stress field disturbance was apparent.

**4.1.1. Flow Rate Control on the Mobility of Gas.** Figure 11(a) shows gas pressure and cumulative average magnitude evolution with time from stages [A] to [F]. In addition, the temporal distribution of positive and negative stress perturbation events is shown (Figure 11(b)). By comparison, a number of features are apparent.

The majority of stress field disturbance during this period appears to have been dominated by microfracture closing events, indicated by a negative polarity. However, it should be noted that the total amount of activity was relatively low between stages [A] to [F], as might be expected given that a quasi-steady-state flow condition had already been reached before stage [A] and continued until the shut-in phase at stage [D]. Perhaps, because of this, no noticeable correlation was observed between the number or magnitude of stress perturbation events and the applied flow rate during stages [A]–[D]. This would seem to indicate that once a quasi-stable microfracture network has been developed, changes in gas flow rate (within the range tested) can be accommodated by variation in the gas pressure and/or aperture of the established gas flow pathways, rather than the propagation of additional pathways.

During stage [D], gas flow was negligible, but a small number of stress fluctuations continued, most likely resulting from the ongoing response of the microfracture network to the decline in gas pressure. Stage [E] marked the reinitiation of gas pumping at a constant flow rate. However, pathway “closure” behaviour was still dominant during this phase, indicating that work was required in order to stimulate the microfracture network after shut-in occurred. Early into stage [F], a peak in gas pressure was observed, which correlated with the reinitiation of the outflow event at radial flow array 3 (Section 3, Figure 2(d)). At the same time, Figures 11(a) and 11(b) indicate a period of increased “opening” type behaviour, which is consistent with the generation of new pathways, or the reopening of preexisting ones, enabling the observed outflow of gas. This would explain the lack of similarity between stages [A] to [C] and [E] to [G]. Controls on differing behaviour may include the degree and distribution of residual gas in the sample and the rate and degree of pathway sealing. As such, one may expect both reopening of old pathways and the creation of new ones during repressuration. This is consistent with observations at field-scale [35] where gas flow rates are seen to temporally and spatially evolve during gas injection.

**4.1.2. Influence of Boundary Condition on the Stability of Gas Pathways.** Stress perturbation data indicate that during stages [G] to [H], there is no evidence for pathway opening, and pathway closure is predominant throughout (Figure 12). This suggests that, while the gas flow network may continue to evolve somewhat under constant pressure, there is no evidence for its continued growth when gas flow is occurring and the system is not energised by an increasing gas pressure.

Similar behaviour is noted in stage [I], which is dominated by pathway closure events, with only one positive event occurring. It may be that this latter event is the consequence of the rapid variations in gas pressures resulting from the constant flow condition. However, it is worth noting that, where a flow pathway (in this case to radial flow array 3) has been established, stress field data indicates that very little propagation of new pathways is necessary, in spite of the gas pressure boundary condition applied.

**4.1.3. Stimulation of the Microfracture Network.** The stress field behaviour observed during stages [J] and [K] differs significantly from previous test stages (Figure 13) in that (a) a greater number of perturbation events were detected in stage [J] (4 times more than in stages [A] to [F]), (b) a significant number of positive events were detected, indicating crack “opening” type behaviour, which dominated early in stage [J], (c) a rapid decline in detected events occurring towards the end of stage [J] and continuing rapidly into stage [K], and (d) the near complete cessation of stress field disturbance by the end of stage [K]. These observations are consistent with gas pressure and outflow data (Figure 6).

The isolation of radial array 3 at the beginning of stage [J] was followed by a sudden increase in positive events (Figure 13(a)), which was quickly countered by a much larger number of negative events (Figure 12(b)). This latter burst of activity also correlated with the onset of gas outflow at radial

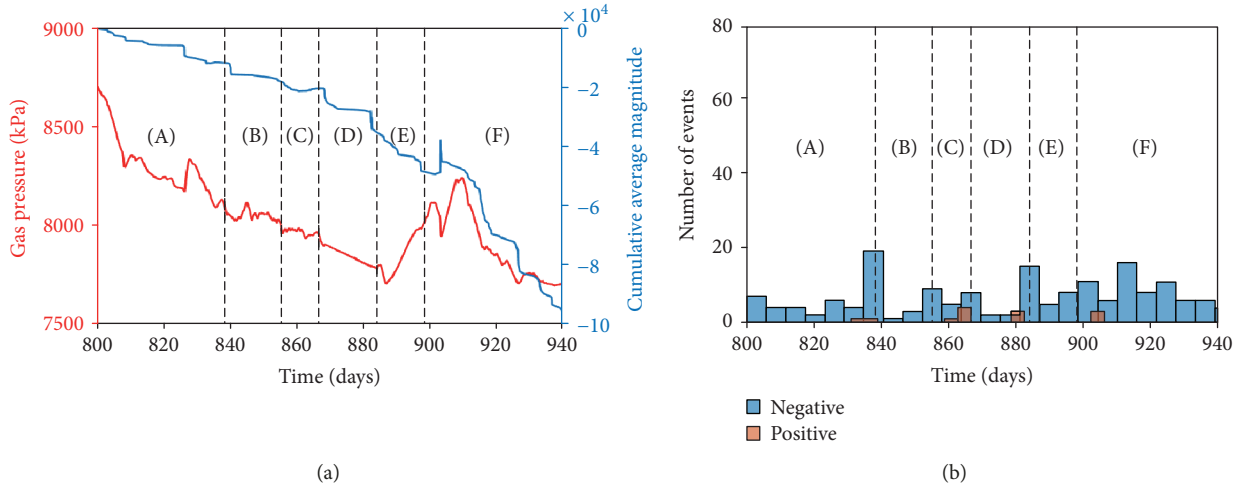


FIGURE 11: Gas pressure and stress field perturbation data from days 800 to 940: (a) evolution of gas pressure and cumulative average magnitude of stress perturbation events with time and (b) temporal distribution of positive and negative stress perturbations.

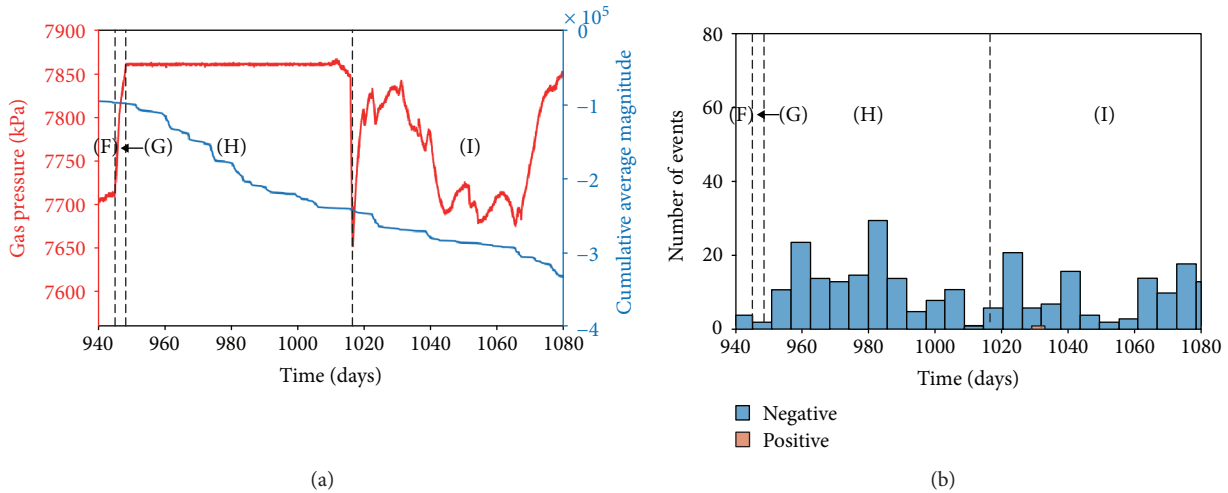


FIGURE 12: Gas pressure and stress field perturbation data from days 940 to 1080: (a) evolution of gas pressure and cumulative average magnitude of stress perturbation events with time and (b) temporal distribution of positive and negative stress perturbations.

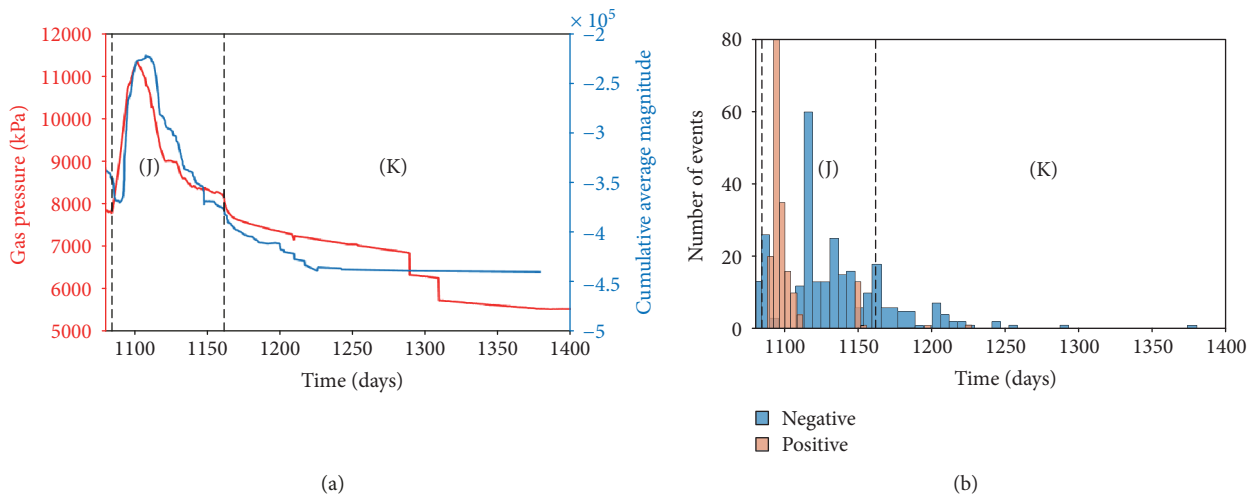


FIGURE 13: Gas pressure and stress field perturbation data from days 1080 to 1400: (a) evolution of gas pressure and cumulative average magnitude of stress perturbation events with time and (b) temporal distribution of positive and negative stress perturbations.

flow array 2. These observations can be explained well by the propagation of new gas pathway/s, stimulated by the closure of the previous route for gas outflow and resulting in gas breakthrough at a different filter array. Nevertheless, this period of microfracture network growth appears to have been short-lived and is followed by the rapid reduction in opening events and a large spike in the number of closure events. This change in behaviour appears to correlate with the onset of outflow to radial flow array 1 (Figure 6(b)), suggesting that gas pressure was relieved sufficiently by this to lead to the closure in one or several pathways before a more stable phase of outflow could be reached.

Stress perturbation data during stage [J] therefore suggest that the generation of new pathways can be instigated by removing access to the outflow filter, requiring the gas to develop a new route for migration. It also indicates that even after outflow is achieved, a period of microfracture network development may continue until quasi-steady-state flow can be reached.

In addition, the rapid reduction in the number of detected stress field perturbations resulting after gas pressure is allowed to decay (stage [K]) suggests that these pathways will close and eventually cease to evolve, in the absence of a constant gas pressure condition. However, it should be noted that these closures continue for long after the system outflow becomes negligible. One explanation for this behaviour may be the final dispersion and redistribution of residual gas within the remaining network.

*4.2. Discussion: Implications.* The primary focus of the experimental programme described in this paper is in essence an examination of gas pathway stability and the impact of gas pressure gradient, the role of boundary condition (constant flow rate or constant pressure), and changes in drainage configuration on a preestablished network of pathways.

The stress analysis approach is able to detect the mechanical disturbance caused by the opening and closure of gas pathways. While some smaller events may not be detected, a clear correlation is observed between applied gas pressure and ongoing stress disturbances (Figure 13(a)). This technique provides valuable insight into the degree of ongoing microfracture opening versus closure, though it should be acknowledged that the nature of these may involve a mixed mode component to their behaviour. Nevertheless, this form of analysis provides a quantitative framework with which to assess pathway stability.

In an established network of gas conductive pathways, changes in the injection flow rate resulted in decrements in pressure (stages [A] through [C]), which, as a general rule of thumb, suggests that halving the gas flow rate results in roughly equal decrements in gas pressure (Table 3). However, analysis shows relatively little perturbation of the stress field, indicating that gas flow is maintained within the preexisting network of microfractures, with very little evolution necessary. While this is contrary to findings demonstrating instability in idealised parallel plate models [18], the influence of scale will also play a role, with the contribution of multiple pathways being the probable cause for the observed metastability. From a repository perspective, the extent of the

zone of metastability and the impact of pathway length scale are yet to be understood. However, on the laboratory scale, the observations presented here would seem to indicate that once a network of pathways is established, they will remain in a metastable state, unless perturbed in some way.

After the injection of gas was halted (stage [D]), gas pressure had to be increased (stage [E]) in order to reestablish outflow. This led to a peak in gas pressure at 8.15 MPa, compared to the 9.48 MPa which was associated with the initiation of gas entry in the intact clay ([17]; stage [11]). Once gas outflow was reestablished, discharge occurred to the same array as that in stages [A] to [C]. The most likely explanation for this is the retention of residual gas within localised regions of the clay following pathway sealing. In a repository, this behaviour would imply that even if gas flow is temporarily halted, the system is capable of returning to a similar metastable state should gas pressures begin to elevate again. Such a return may be achieved more rapidly if sufficient residual gas remains within the network. However, it is important to consider the impact of rehydration and the diffusion of gas from localised zones within the clay which, over time, may reduce this residual memory and return the clay to its intact properties.

Once flow is restarted, by varying the boundary condition, the system is observed to self-regulate, as evidenced by (i) fluctuations in flow to maintain a constant injection pressure (stage [H]), (ii) fluctuations in gas pressure to maintain a constant flow rate (stage [I]), and (iii) minimal evidence for opening of new pathways detected in the stress field analysis (stages [H] and [I]). This suggests variation in aperture is sufficient to maintain flow without significant propagation of new pathways. This further indicates a significant degree of short term stability in these microfracture networks.

Assuming long-term changes in repository conditions, the availability of drainage points may vary. During experimental testing (stage [J]), the removal of the drainage path to radial array 3 led to a rapid redevelopment of the microfracture network as shown by the stress event analysis and changes in the outflow distribution. Since multiple independent pore pressure measurements were available (EC-1, EC-2, and radial array 3), we were able to directly measure the internal gas pressure within the network. At the scale of testing, it is therefore apparent that a negligible pressure drop exists between the injection filter and these points of measurement. This suggests that the internal volume of the microfracture network must be substantially smaller than the injection reservoir. Furthermore, where drainage occurs, the capillary pressure drop must be very steep in the vicinity around the drain/filter.

This phase of testing was also marked by a period of major stress field disturbance and evidence for microfracture opening, which can be explained by the propagation of new pathways to radial arrays 1 and 2. This led to a peak gas pressure of 11.35 MPa compared to the 9.88 MPa which was associated with the development of the original network of gas pathways ([17]; stage 11). This implies that the availability of drainage pathways will be a crucial control on the generation of peak gas pressures during advective flow.

As the repository processes leading to gas generation cease, a decline in gas pressure is expected. When these conditions are mirrored, stage [K], a rapid reduction in outflow is accompanied by crack closure. Later, quiescence in the stress field indicates microfracture closure also ceases, suggesting that the clay is returning towards its initial state. In terms of repository performance, this implies a capacity for self-sealing on long timescales.

The total number of stress perturbations and the apparent time dependency of gas network development highlights the complexity in modelling such a system. Intuitively, it seems likely that small changes in initial conditions may result in differing network configurations and hence impact both bulk flow properties and the evolution of gas pressure in a repository. Further work is therefore required to understand the controls governing the spatial distribution of these networks and their evolution on repository timescales.

## 5. Conclusions

A unique experimental dataset is presented examining the stability of an established gas network during advective flow in precompacted bentonite. In such conditions, gas flow is strongly coupled with the stress field experienced by the clay. Within this paper, for the first time, three scenarios are examined: (i) flow rate control on the mobility of gas, (ii) influence of boundary condition on the stability of gas pathways, and (iii) stimulation of the microfracture network. In the first scenario, findings show that relatively little perturbation of the stress field occurs when the rate of gas inflow is varied, indicating that gas flow is primarily maintained within the preexisting network of microfractures. In the second scenario, varying the boundary condition (constant vs. variable gas pressure) resulted in system self-regulation, suggesting variation in aperture is sufficient to maintain flow without significant propagation of new pathways. Finally, the removal of a drainage path resulted in rapid redevelopment of a new microfracture network. This implies that the availability of drainage pathways will be a crucial control on the generation of peak gas pressures in a radioactive waste repository. In addition, observations relating to the cessation of gas flow indicate the potential for crack-closure and self-sealing. Our findings show that an improved knowledge of the distribution characteristics of gas flow networks is necessary to understand their evolution on repository timescales. Without this additional information, uncertainty in the prediction of gas pressure evolution remains.

## Data Availability

The data used to support the findings of this study are available from the corresponding author upon request.

## Additional Points

*Highlights.* Stress perturbation analysis can be used to monitor an evolving gas network. For the first time, controls on the stability of an established network are examined. Gas

pressure can be reconstructed from changes in the internal stress field. Gas flow is controlled by a population of both a few large- and many small-scale events.

## Disclosure

The views expressed herein do not necessarily represent those of the funding organisation.

## Conflicts of Interest

There are no conflicts of interest associated with the publication of the paper. The affiliation of each author is stated as is the funding route for the derivation of the data. Three of the authors work for the BGS and the fourth works for (RWM). No conflicts of interest exist in either the route of funding or the publication of the data.

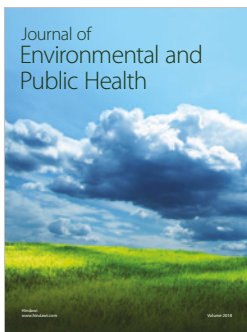
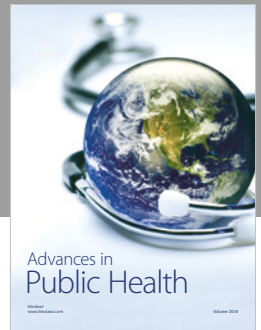
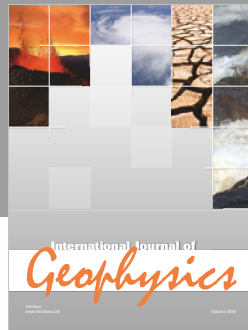
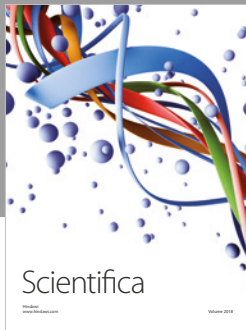
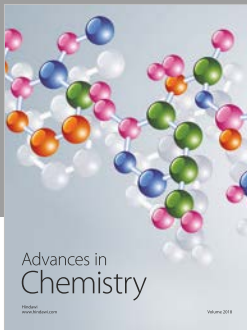
## Acknowledgments

The project was sponsored by the Radioactive Waste Management Ltd. and the British Geological Survey (aligned to the BGS Geosphere Containment Project). Experiments were conducted in the Transport Properties Research Laboratory (TPRL), part of the Fluid Processes Research Group. The authors would also like to thank Mr. Humphrey Wallis and colleagues from the BGS Research & Design workshops who contributed to the design and manufactured the bespoke equipment used in this study and Mrs. Fiona McEvoy and Dr. Elena Tamayo-Mas for their time and constructive comments in the internal review of this paper. This paper is published with permission from the Executive Director of the British Geological Survey.

## References

- [1] W. R. Rodwell, A. W. Harris, S. T. Horseman et al., *Gas Migration and Two-Phase Flow through Engineered and Geological Barriers for a Deep Repository for Radioactive Waste*, European Commission, Report EUR19122EN, 1999.
- [2] B. Bonin, M. Colin, and A. Dutfoy, "Pressure building during the early stages of gas production in a radioactive waste repository," *Journal of Nuclear Materials*, vol. 281, no. 1, pp. 1–14, 2000.
- [3] L. Ortiz, G. Volckaert, and D. Mallants, "Gas generation and migration in Boom Clay, a potential host rock formation for nuclear waste storage," *Engineering Geology*, vol. 64, no. 2–3, pp. 287–296, 2002.
- [4] E. Weetjens and X. Sillen, "Gas generation and migration in the near field of a supercontainer-based disposal system for vitrified high-level radioactive waste," *Proceedings of the 11th international high-level radioactive waste management conference (IHLRWM)*, 2006, pp. 1–8, Las Vegas, United States, April 2006.
- [5] R. S. Wikramaratna, M. Goodfield, W. R. Rodwell, P. J. Nash, and P. J. Agg, *A Preliminary Assessment of Gas Migration from the Copper/Steel Canister*, SKB Technical Report TR93–31, 1993.
- [6] J. C. Parker, "Multiphase flow and transport in porous media," *Reviews of Geophysics*, vol. 27, no. 3, p. 311, 1989.

- [7] M. T. van Genuchten, "A closed-form equation for predicting the hydraulic conductivity of unsaturated soils1," *Soil Science Society of America Journal*, vol. 44, no. 5, 1980.
- [8] J. B. Kool and J. C. Parker, "Development and evaluation of closed-form expressions for hysteretic soil hydraulic properties," *Water Resources Research*, vol. 23, no. 1, pp. 105–114, 1987.
- [9] P. H. Nelson, "Pore-throat sizes in sandstones, tight sandstones, and shales," *AAPG Bulletin*, vol. 93, no. 3, pp. 329–340, 2009.
- [10] P. T. Hang and G. W. Brindley, "Methylene blue absorption by clay minerals. Determination of surface areas and cation exchange capacities (clay-organic studies XVIII)," *Clays and Clay Minerals*, vol. 18, no. 4, pp. 203–212, 1970.
- [11] W. S. Abdullah, K. A. Alshibli, and M. S. Al-Zou'bi, "Influence of pore water chemistry on the swelling behavior of compacted clays," *Applied Clay Science*, vol. 15, no. 5-6, pp. 447–462, 1999.
- [12] B. V. Derjaguin, N. V. Churaev, and V. M. Muller, "Surface forces," in *Translated from Russian by V.I. Kisin, J. A. Kitchener, Ed., Consultants Bureau, New York, 1st edition, 2007.*
- [13] C. E. Neuzil, "How permeable are clays and shales?," *Water Resources Research*, vol. 30, no. 2, pp. 145–150, 1994.
- [14] J. J. Wang, J. G. Zhu, C. F. Chiu, and H. Zhang, "Experimental study on fracture toughness and tensile strength of a clay," *Engineering Geology*, vol. 94, no. 1-2, pp. 65–75, 2007.
- [15] J. F. Harrington and S. T. Horseman, "Gas transport properties of clays and mudrocks," *Geological Society, London, Special Publications*, vol. 158, no. 1, pp. 107–124, 1999.
- [16] P. Sellin and O. X. Leupin, "The use of clay as an engineered barrier in radioactive-waste management—a review," *Clays and Clay Minerals*, vol. 61, no. 6, pp. 477–498, 2013.
- [17] J. F. Harrington, C. C. Graham, R. J. Cuss, and S. Norris, "Gas network development in a precompacted bentonite experiment: evidence of generation and evolution," *Applied Clay Science*, vol. 147, pp. 80–89, 2017.
- [18] P. Persoff and K. Pruess, "Two-phase flow visualization and relative permeability measurement in natural rough-walled rock fractures," *Water Resources Research*, vol. 31, no. 5, pp. 1175–1186, 1995.
- [19] M. Angeli, M. Soldal, E. Skurtveit, and E. Aker, "Experimental percolation of supercritical CO<sub>2</sub> through a caprock," *Energy Procedia*, vol. 1, no. 1, pp. 3351–3358, 2009.
- [20] R. J. Cuss and J. F. Harrington, *Update on Dilatancy Associated with Onset of Gas Flow in Callovo-Oxfordian Claystone. Progress Report on Test SPP\_COx-2*, British Geological Survey commissioned report CR/11/110, 2011.
- [21] G. Mandl and R. M. Harkness, "Hydrocarbon migration by hydraulic fracturing," *Geological Society, London, Special Publications*, vol. 29, no. 1, pp. 39–53, 1987.
- [22] P. Marschall, S. Horseman, and T. Gimmi, "Characterisation of gas transport properties of the Opalinus Clay, a potential host rock formation for radioactive waste disposal," *Oil & Gas Science and Technology*, vol. 60, no. 1, pp. 121–139, 2005.
- [23] E. Skurtveit, E. Aker, M. Soldal, M. Angeli, and E. Hallberg, *Influence of Micro Fractures and Fluid Pressure on Sealing Efficiency of Caprock: A Laboratory Study on Shale, Conference on Greenhouse Gas Technologies (GHGT) 10*, RAI Amsterdam, The Netherlands, 2010.
- [24] E. Skurtveit, E. Aker, M. Soldal, M. Angeli, and Z. Wang, "Experimental investigation of CO<sub>2</sub> breakthrough and flow mechanisms in shale," *Petroleum Geoscience*, vol. 18, no. 1, pp. 3–15, 2012.
- [25] B. Tissot and R. Pellet, "Nouvelles données Sur les mécanismes de genèse et de migration du pétrole: Simulation mathématique et application à la prospection," in *Proceedings of the 8th world Petroleum congress*, pp. 35–46, Moscow, 1971.
- [26] P. Sellin, "Gas migration in bentonite—fundamental issues," in *FORGE FP7 WP3 Final Report D3.38: Experiments and Modelling on the Behaviour of EBS*, Published by the European Commission, 2014.
- [27] L.-E. Johannesson, *Manufacturing of Buffer and Filling Components for the Multi Purpose Test*, SKB P-14-07, Svensk Kärnbränslehantering AB, 2014.
- [28] C. C. Graham, J. F. Harrington, and R. J. Cuss, "Gas migration in bentonite - fundamental issues," in *Experiments and modelling on the behaviour of EBS*, vol. 38, pp. 232–255, FORGE Report D3, 2014.
- [29] S. T. Horseman, J. F. Harrington, and P. Sellin, "Gas migration in clay barriers," *Engineering Geology*, vol. 54, no. 1-2, pp. 139–149, 1999.
- [30] C. C. Graham, J. F. Harrington, R. J. Cuss, and P. Sellin, "Gas migration experiments in bentonite: implications for numerical modelling," *Mineralogical Magazine*, vol. 76, no. 8, pp. 3279–3292, 2012.
- [31] R. J. Cuss, J. F. Harrington, D. J. Noy, C. C. Graham, and P. Sellin, "Evidence of localised gas propagation pathways in a field-scale bentonite engineered barrier system; results from three gas injection tests in the large scale gas injection test (Lasgit)," *Applied Clay Science*, vol. 102, pp. 81–92, 2014.
- [32] C. C. Graham, S. Stanchits, I. G. Main, and G. Dresen, "Comparison of polarity and moment tensor inversion methods for source analysis of acoustic emission data," *International Journal of Rock Mechanics and Mining Sciences*, vol. 47, no. 1, pp. 161–169, 2010.
- [33] A. Zang, F. Christian Wagner, S. Stanchits, G. Dresen, R. Andresen, and M. A. Haidekker, "Source analysis of acoustic emissions in Aue granite cores under symmetric and asymmetric compressive loads," *Geophysical Journal International*, vol. 135, no. 3, pp. 1113–1130, 1998.
- [34] C. C. Graham, J. F. Harrington, and P. Sellin, "Gas migration in pre-compacted bentonite under elevated pore-water pressure conditions," *Applied Clay Science*, vol. 132-133, pp. 353–365, 2016.
- [35] R. Cuss, J. Harrington, C. Graham, and D. Noy, "Observations of pore pressure in clay-rich materials; implications for the concept of effective stress applied to unconventional hydrocarbons," *Energy Procedia*, vol. 59, pp. 59–66, 2014.
- [36] L. Börgesson, O. Karnland, and L.-E. Johannesson, "Modelling of the physical behaviour of clay barriers close to water saturation," *Engineering Geology*, vol. 41, no. 1-4, pp. 127–144, 1996.



**Hindawi**

Submit your manuscripts at  
[www.hindawi.com](http://www.hindawi.com)

